Surface-Charge-Dependent Cell Localization and Cytotoxicity of Cerium Oxide Nanoparticles

Atul Asati,[†] Santimukul Santra,[†] Charalambos Kaittanis,[†,‡] and J Manuel Perez[†,‡,§,*]

[†]NanoScience Technology Center, Suite 400, 12424 Research Parkway, Orlando, Florida 32826 and [‡]Burnett School of Biomedical Sciences, College of Medicine and [§]Department of Chemistry, University of Central Florida, Orlando, Florida 32826

ABSTRACT Cerium oxide nanoparticles (nanoceria) have shown great potential as antioxidant and radioprotective agents for applications in cancer therapy. Recently, various polymer-coated nanoceria preparations have been developed to improve their aqueous solubility and allow for surface functionalization of these nanoparticles. However, the interaction of polymer-coated nanoceria with cells, their uptake mechanism, and subcellular localization are poorly understood. Herein, we engineered polymer-coated cerium oxide nanoparticles with different surface charges (positive, negative, and neutral) and studied their internalization and toxicity in normal and cancer cell lines. The results showed that nanoceria with a positive or neutral charge enters most of the cell lines studied, while nanoceria with a negative charge internalizes mostly in the cancer cell lines. Moreover, upon entry into the cells, nanoceria is localized to different cell compartments (*e.g.*, cytoplasm and lysosomes) depending on the nanoparticle's surface charge. The internalization and subcellular localization of nanoceria plays a key role in the nanoparticles' cytotoxicity profile, exhibiting significant toxicity when they localize in the lysosomes of the cancer cells. In contrast, minimal toxicity is observed when they localize into the cytoplasm or do not enter the cells. Taken together, these results indicate that the differential surface-charge-dependent localization of nanoceria in normal and cancer cells plays a critical role in the nanoparticles' toxicity profile.

KEYWORDS: polymer-coated nanoceria · nanoparticle cell uptake · cerium oxide · nanotoxicity · lysosomal uptake

Nanomaterials with unique magnetic, luminescent, and catalytic properties are being engineered for numerous biomedical applications, including imaging, diagnostics, and therapy.[1−7] However, nanomaterial's greatest strength, which relies primarily on the enhanced physical and chemical characteristics that matter exhibits at this scale, has the potential to be its greatest liability. Potentially harmful interactions can occur between nanomaterials and living systems, including humans. For this reason, nanomaterials must be engineered using materials that are either nontoxic, biocompatible, and biodegradable or that have minimal and in some cases beneficial properties. An inflammatory response is a parameter that is often investigated to assess the effect that nanomaterials have within an organism.[8] For instance, recent studies have shown that titanium oxide nanoparticles, which are widely used in cosmetics and skin care products, can elicit an inflammatory response and generation of reactive oxygen species, causing DNA damage.[9] Also, single-walled carbon nanotubes can cause lipid peroxidation, oxidative stress, mitochondrial dysfunction, and changes in cell morphology upon *in vitro* incubation with keratinocytes and bronchial epithelial cells.[10,11] Furthermore, silver nanoparticles have been found to display size-dependent toxicity when exposed to alveolar macrophages *via* induction of oxidative stress,[12,13] while quantum dots and fullerenes can also initiate an inflammatory response and generation of reactive oxygen species.[14−16]

Cerium oxide nanoparticle (nanoceria) is a unique nanomaterial because it exhibits anti-inflammatory properties. Nanoceria has been found to scavenge reactive oxygen spe-
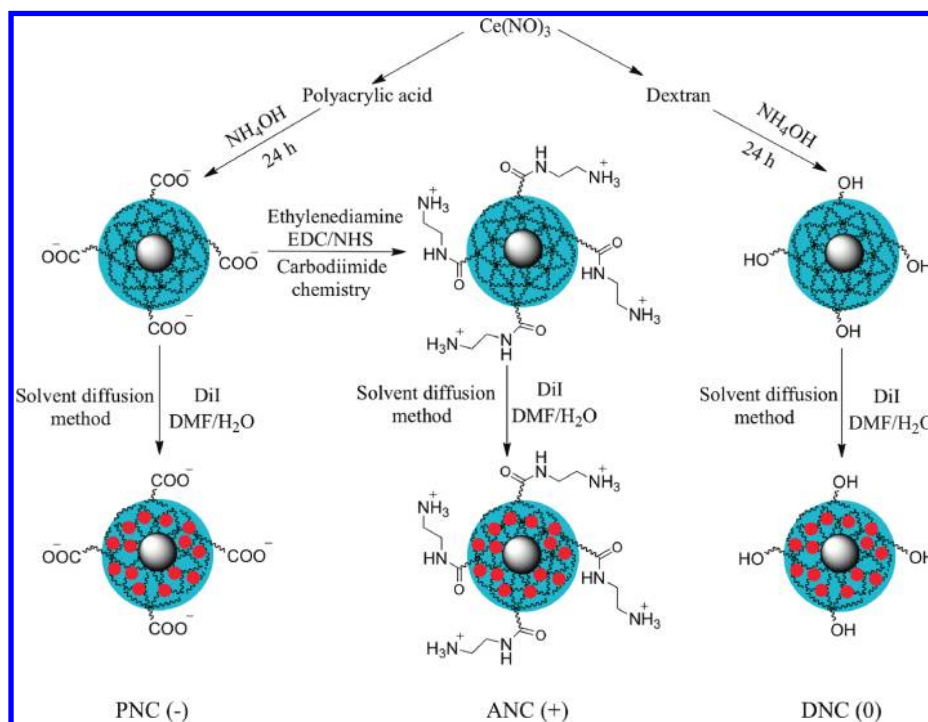
cies (ROS), possess superoxide-dismutase-like activity, prevent cardiovascular myopathy, and provide radioprotection to normal cells from radiation.[17−21] We recently reported the synthesis of biocompatible polymer-coated nanoceria with enhanced aqueous stability and unique pH-dependent antioxidant activity.[17] In particular, we have found that nanoceria displays optimal antioxidant properties at physiological pH, whereas it behaves as an oxidase at acidic pH.[22] Hence, this selective behavior may explain nanoceria's selective cytoprotection to normal cells but not to cancer cells during radiation treatment or oxidative stress.[20] In addition, the nature of the polymeric coating surrounding the cerium oxide core could play a critical role in nanoceria's beneficial (antioxidant) *vs* harmful (oxidant) properties. We also reasoned that the cytotoxicity of cerium oxide nanoparticles could depend upon their

Scheme 1. Surface functionalization of cerium oxide nanoparticles cerium oxide nanoparticles with different polymer coatings and surface modifications were synthesized to yield nanoparticles with negative [PNC(−)], positive [ANC(+)], and neutral [DNC(0)] charge. A fluorescent dye (DiI, red circle) was encapsulated using a modified solvent diffusion method.

subcellular localization. Once inside the cells, the nanoparticle's toxicity could depend on whether they are localized in particular cellular organelles, such as the lysosomes (which are acidic), or distributed in the cytoplasm (which is at neutral pH in normal cells). In addition, since most tumors have an acidic microenvironment, this might switch off nanoceria's antioxidant activity, turning on its oxidase activity and consequently sensitizing the tumor toward radiation therapy.

In this work, we report the polymer's surface-charge-dependent cell internalization and cytotoxicity profile of cerium oxide nanoparticles in normal vs malignant cells. We selected various cell lines in order to assess the corresponding behavior of cerium oxide nanoparticles. Cardiac myocytes (H9c2) and human embryonic kidney (HEK293) cells were selected as nontransformed (normal) cells, whereas lung (A549) and breast (MCF-7) carcinomas were selected as transformed (cancer) cell lines. Results showed that positively charged nanoceria internalized in all cells except for the breast carcinoma, localizing preferentially in the lysosomes and subsequently becoming toxic to these cells. In contrast, nanoceria with a negative charge was internalized only by lung carcinoma (A549) cells but not by the breast carcinoma cells (MCF-7), thus exhibiting toxicity only to the lung carcinoma cells. Notably, the negative charged nanoceria localized into the lysosomes of the A549 cells, while they were not internalized and therefore were not toxic to the normal cells (either cardiac myocytes or human embryonic kidney cells). Surprisingly, nanoceria with neutral charge was not toxic to normal cells or cancer cells, as these nanoparticles primarily localized in the cytoplasm of these cells. Taken together, our results suggest that the internalization and subcellular localization of polymer-coated nanoceria plays a critical role in the toxicity profile of this nanomaterial. Our results also suggest that the coating on nanoceria can be engineered in order to modulate its differential cytotoxicity behavior in cancer vs normal cells.

RESULTS

Synthesis and Characterization of Polymer-Coated Cerium Oxide Nanoparticles. For our studies, we synthesized various nanoceria preparations coated with either poly(acrylic acid) (PNC), aminated poly(acrylic acid) (ANC), or dextran (DNC) (Scheme 1), endowing our nanoparticles with a negative (−), positive (+), or neutral (0) surface charge, respectively. Transmission electron microscopy (TEM) studies showed the presence of nanoparticles of similar core size (3−4 nm) in all preparations as reported previously[22] (Figure 1a). Dynamic light-scattering experiments showed the presence of monodisperse nanoceria preparations with an average hydrodynamic diameter of 14 nm for DNC(0) and 5 nm for both PNC(+) and ANC(−) (see the Supporting Information, Figure S1). The presence of different surface charges in the various nanoceria preparations was assessed by ζ potential (Figure 1b), confirming the presence of a negative, neutral, and positive charge for PNC, DNC, and ANC, respectively. FT-IR analysis further confirmed the nanoparticle's polymer surface coating and functionality (Figure 1c). During synthesis, we fluores-
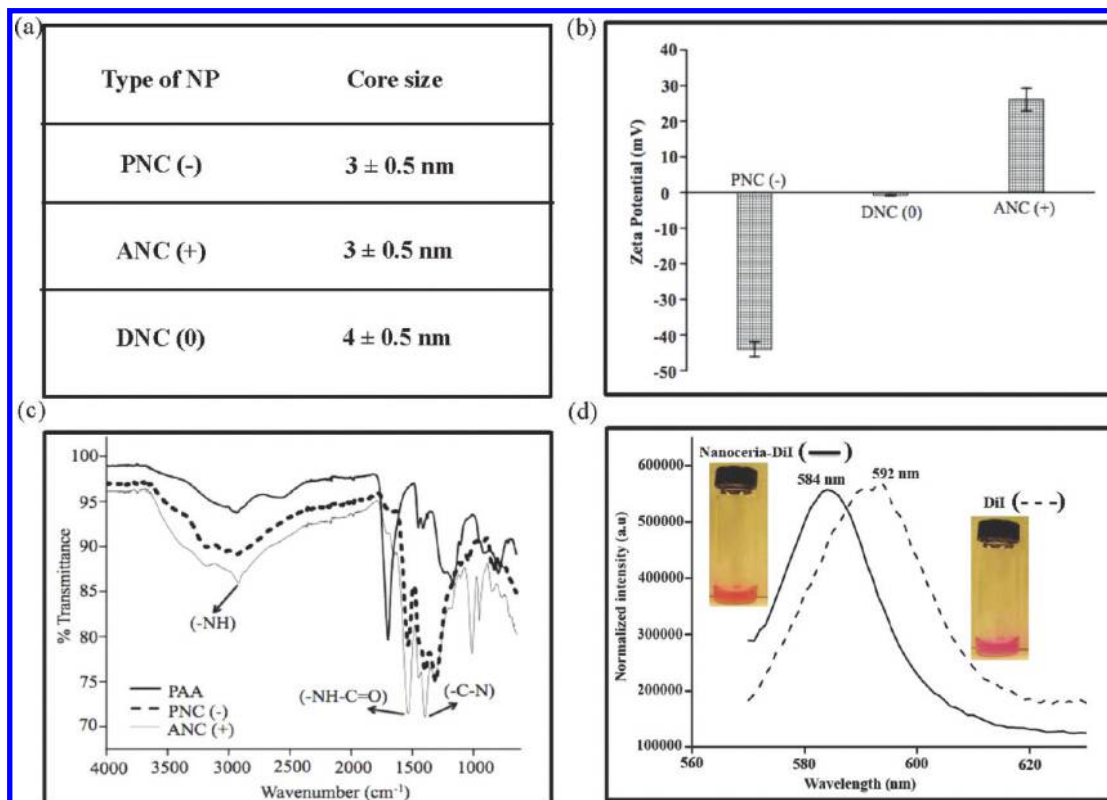
Figure 1. Characterization of cerium oxide nanoparticles. (a) Size of cerium oxide nanocrystal core by TEM. (b) ζ potential of cerium oxide nanoparticles with different surface functionalities (negative, neutral, and positive). (c) FT-IR spectra of the carboxylated (negative) and aminated (positive) surface group on nanoceria. (d) Fluorescence emission spectra of the DiI-encapsulating nanoceria and free dye DiI.

cently labeled the nanoparticles by encapsulating a dye (DiI) within the hydrophobic microdomains of the polymeric coatings of each nanoceria preparation, following a previously reported methodology.[23] Therefore, using this approach, we introduced fluorescent modality to the polymer-coated nanoceria, without compromising the solubility of the nanoparticles in aqueous media or reducing the number of available functional groups on the nanoparticle surface. Successful encapsulation of DiI into the nanoceria was confirmed *via* fluorescence spectroscopy, where a blue shift in the DiI-encapsulating ceria nanoparticles (584 nm) emission spectrum was observed as opposed to DiI alone (592 nm) (Figure 1d). The DiI-encapsulating polymer-coated-nanoceria displayed good aqueous stability over long periods of time without significant release of the dye and can be used for the intracellular tracking of the nanoparticles.

Nanoceria's Surface-Charge-Dependent Cellular Interaction. Confocal microscopy experiments were performed in order to study the cellular uptake and intracellular localizaton of the DiI-labeled polymer-coated nanoceria. In these experiments, PNC(−), ANC(+), and DNC(0) (1.0 mM) were incubated with two transformed carcinoma cell lines (A549 lung and MCF-7 breast carcinomas) and two nontransformed (normal) cell lines (H9c2 cardiac myocytes and HEK293 human embryonic kidney cells). We selected these cell lines in order to investigate if

they differently uptake the ANC(+), PNC(−), and DNC(0) nanoparticles, thus potentially displaying different toxicity profiles.

First, we studied the internalization pattern of ANC(+), PNC(−), and DNC(0) in the two normal cells [HEK293 and H9c2 (10000 cells)] (Figure 2). After a 3 h incubation, results showed that the negatively charged carboxylated nanoparticles [PNC(−)] were minimally uptaken by the HEK293 cells and did not internalize in the H9c2 cell line. Meanwhile, the positively charged aminated nanoparticles [ANC(+)] were uptaken by both cells, with the H9c2 cardiac myocytes uptaking more nanoparticles than the HEK293 human embryonic kidney cells, as indicated by the elevated cell-associated fluorescence in the H9c2 cells. The neutral dextran-coated nanoparticle [DNC(0)] was internalized by both cell lines, although a higher degree of internalization was observed in the H9c2 as opposed to the HEK293. Interestingly, the DNC(0) intracellular fluorescence pattern (particularly in the H9c2 cells) was diffused, being different from the ANC(+)-punctuated fluorescence pattern. This difference seems to indicate a unique nanoparticle surface-charge dependent internalization mechanism with different intracellular compartmentalization among the nanoparticles studied and these two nontransformed cell lines.

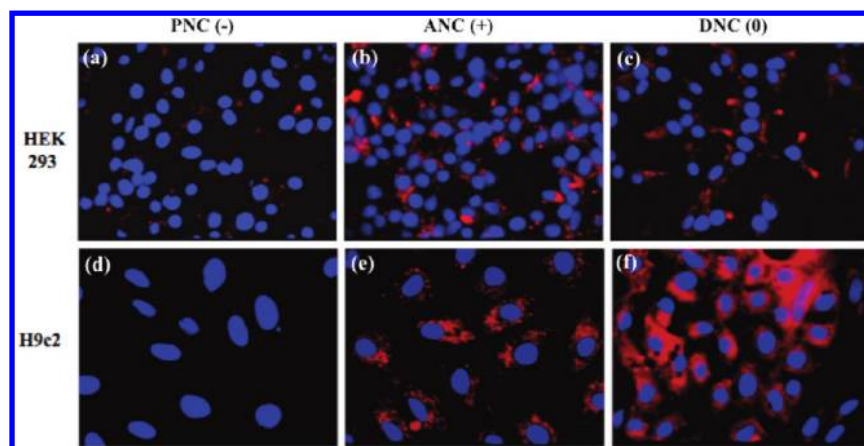Internalization experiments preform with cancer cells (10000 cells) derived from lung (A549) and breast

Figure 2. Uptake of cerium oxide nanoparticles (nanoceria) by normal cells *via* confocal microscopy. PNC(−) is not being significantly uptaken by either cell line (a, d), whereas uptake is observed with the ANC(+) (b, e). DNC(0) exhibits diffused cytoplasmic localization (c, f) with greater internalization in H9c2.

(MCF-7) carcinomas revealed PNC(−) uptake by the A549 cells but no uptake by the MCF-7 cells (Figure 3). In contrast, both cell lines were able to uptake ANC(+). Interestingly, a higher degree of internalization and pronounced punctuated fluorescence was observed with the ANC(+) in the A549 cells. This might indicate that in these cells the majority of the ANC(+) localized into endosomal compartments. In contrast, minimal and diffused intracellular fluorescence was observed with the DNC(0) in both the A549 and MCF-7 cells, suggesting that these nanoparticles are mostly localized in the cytosol with a small fraction confined within the endosomal compartments. Taken together, the above results suggest that the surface charge on polymer-coated nanoceria dictates their differential internalization and localization in normal *vs* cancer cells (Figures 2 and 3, respectively).

Cellular Mechanism of Nanoparticle Uptake. To further investigate the mechanism of cellular uptake and verify if the endocytic pathway is responsible for the internalization of polymer-coated nanoceria, we performed a series of experiments at 4 °C and with endocytic inhibitors [2-deoxyglucose (50 mM) and sodium azide (10

mM)]. For instance, at 4 °C the endocytic/pinocytic mechanism is arrested.[24−26] Thus, after incubating cells (10000 cells) with the various DiI-labeled nanoceria preparations (1.0 mM) at 4 °C, we observed negligible nanoparticle internalization (Figure 4a−c). Since none of the polymer-coated nanoceria entered the A549 lung carcinoma or H9c2 cardiac myocytes cells, it was suggested that endocytosis is a possible mechanism of internalization in all cases. Experiments performed at 37 °C in the presence of 2-deoxyglucose and sodium azide confirmed our results (Figure 4d−f). Specifically, both A549 and H9c2 cells did not uptake the DiI-labeled nanoceria [PNC(−), ANC(+), or DNC(0)] in the presence of these inhibitors as expected. These results confirm that these nanoparticles were actively uptaken by an endocytic process. Since PNC(−) were not significantly uptaken by the H9c2 cells, experiments using these cells at 4 °C or in the presence of inhibitors were not performed.

Intracellular Distribution of Polymeric Cerium Oxide Nanoparticles. To corroborate that after internalization some of the polymer-coated nanoceria localized in endosomal compartments, we first treated the cells
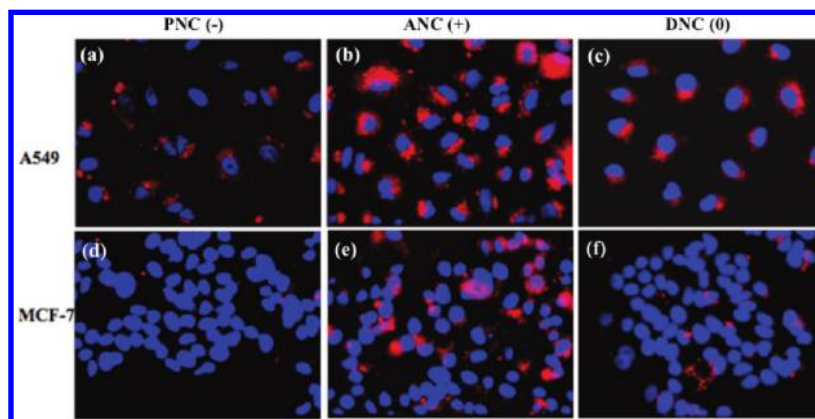

Figure 3. Uptake of cerium oxide nanoparticles (nanoceria) by cancer cells. Confocal images of A549 and MCF-7 carcinoma cells after treatment with PNC(−), ANC(+), and DNC(0) for 3 h. PNC(−) (a,d) are being uptaken by A549 and not by MCF-7 cells, while ANC(+) (b,e) are being uptaken by both cell lines. Meanwhile, DNC(0) internalized in the A549 (c), while they were minimally internalized by MCF-7 (f).
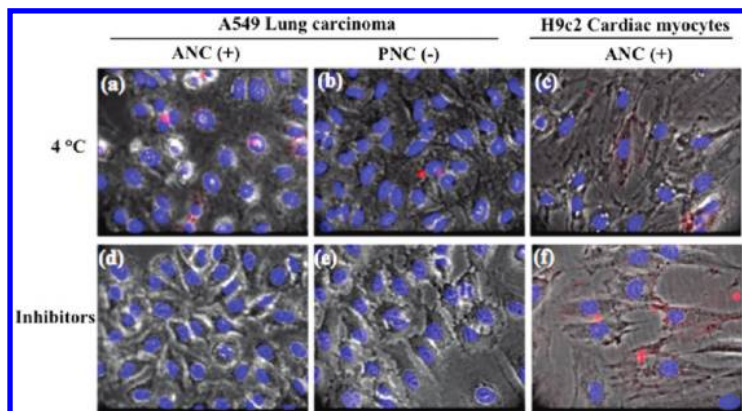
Figure 4. Inhibition of endocytic pathways prevents nanoceria uptake. No internalization of ANC(+) and PNC(−) is seen in both cell lines at 4 °C (a−c). Similarly, internalization of the nanoparticles is abrogated in the presence of inhibitors (2-deoxyglucose and sodium azide), which collectively block active endocytosis (d−f).

(10000 cells) for 3 h with the PNC(−), ANC(+), and DNC(0) (1.0 mM) followed by a 20 min treatment with Lysotracker (35 nM), a lysosome-specific dye. Lysotracker is a green fluorescent dye that stains the acidic lysosomes; hence, the potential colocalization between DiI-labeled-nanoceria (red) and lysosomes (green) should yield a yellow/orange overlap when the images are merged. Experiments were carried out with A549 lung carcinoma cells and H9c2 cardiac myocytes. Results showed that DiI-labeled-ANC(+) and DiI-labeled-PNC(−) colocalized with Lysotracker in the A549 lung cancer cells, as determined by confocal microscopy (Figure 5a−f and Figure S2, Supporting Information). Even though less internalization of DiI-labeled-PNC(−) is observed in these cells, the internalized nanoparticles predominantely colocalized with the Lysotracker dye indicating lysosomal localization. In contrast, DiI-labeled-DNC(0) showed a diffused distribution with minimal localization in the lysosomes of A549 cells (Figure 5g−i and Figure S3, Supporting Information). Interestingly, in the case of H9c2 cardiac myocytes, the distribution of DiI-labeled-ANC(+) inside the cell colocalized mostly with the Lysotracker marker (Figure 6a−c and Figure S3, Supporting Information). Meanwhile, when the DiI-labeled-DNC(0) was used, a diffused distribution of internalized nanoparticles (DiI signal) was observed with minimal colocalization with the lysosomes (Figure 6d−f and Figure S3, Supporting Information). This indicates that in H9c2 cardiac myocytes, the neutral DiI-labeled-DNC(0) primarily localizes to the cytosol while the DiI-labeled-ANC(+) localized to the lysosome. Lysosomal colocalization experiments were not done using H9c2 and DiI-labeled PNC(−) since these nanoparticles are not uptaken by these cells (Figure 2). These results demonstrate that the surface charge on the ceria nanoparticles dictates the nanoparticles' subcellular localization in cancer and normal cells.

Determination of the Oxidase-Like Activity of Lysosome-Residing Nanoceria.
Nanoceria has been reported to possess unique oxidase-like activity at acidic pH, oxidizing various colorimetric substrates, such as 3,3′,5,5′-tetramethylbenzydine (TMB) and 2,2-azinobis(3-ethylbenzothizoline-6-sulfonic acid (AzBTS).[22] This activity can be employed to assess the localization of nanoceria in various cell organelles, particularly lysosomes, *via* the nanoparticle's oxidase activity, using TMB as the colorimetric substrate. Hence, to further confirm that some of the polymer-coated cerium oxide nanoparticles localized into the lysosomes, cells were incubated with the different nanoceria preparations for 3 h, followed by lysosomal isolation. Then, the oxidase activity of the isolated lysosomes was determined spectrophotometrically *via* TMB oxidation. As expected and in agreement with the microscopy and lysosomal colocalization experiments, we found that ANC(+) were mostly entrapped within the lysosome of the H9c2, HEK293, and A549 cell lines, as the lysosomes isolated from these cells exhibited significant levels of oxidase activity (Figure 7a−c). In MCF-7 breast carcinoma cell line, no localization to the lysosomes was observed as these cells do not uptake any of the nanoparticles (Figure 7d). Interestingly, when cells were incubated with PNC(−), only the lysosomes isolated from A549 lung carcinoma cells exhibited oxidase activity as expected on the basis of the lysosomal colocalization experiments. Meanwhile, the lysosomes from cells incubated with the DNC(0) exhibit minimal oxidase activity, corroborating
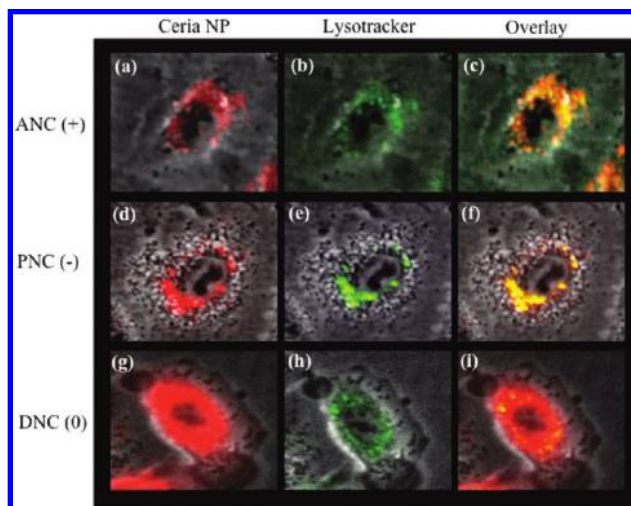

Figure 5. Polymer-coated nanoceria's intracellular localization in lung carcinoma cells (A549). Upon internalization, both the positively charged [ANC(+), a−c] and negatively charged [PNC(−), d−f] nanoceria colocalized with the lysosome. In contrast, neutral nanoceria [DNC(0), g−i] localized mostly in the cytoplasm.
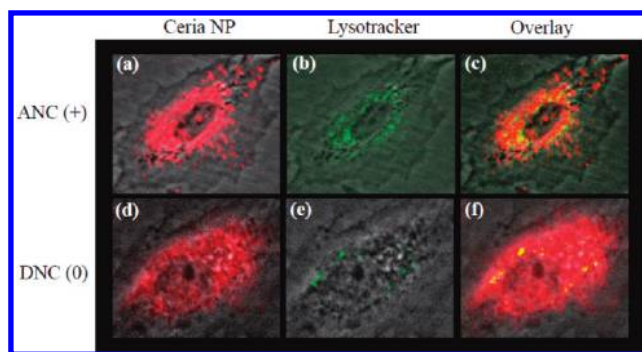
Figure 6. Polymer-coated nanoceria's intracellular localization in cardiac myocytes (H9c2). Upon internalization, the positively charged [ANC(+), a−c] nanoceria is found in both the cytoplasm and lysosomes. In contrast, neutral nanoceria [DNC(0), d−f] does not significantly colocalize to the lysosomes with most of the nanoparticles found in the cytoplasm.

the confocal microscopy studies. Lysosomes isolated from untreated cells (H9c2, HEK293, A549, and MCF-7) did not possess any oxidase activity (control), as indicated by the absence of TMB oxidation (Figure 7) and confirming the absence of endogenous oxidase activity in these organelles.

Intracellular-Distribution-Dependent Cytotoxicity of Polymeric Cerium Oxide Nanoparticles. In order to determine if the surface-charge-dependent internalization and intracellular (lysosomal *vs* cytoplasmic) localization of the polymeric nanoceria plays a role in the nanoparticle's cytotoxicity, cell viability (MTT) assays were performed. Interestingly, we found that DNC(0) did not exhibit any toxicity to the cell lines studied (Figure 8), as most of these nanoparticles localized to the cytoplasm. Further-

more, prolonged incubation of these cell lines with the dextran-coated-nanoceria did not affect cell morphology and proliferation ability as previously reported.[17] In contrast, ANC(+) and PNC(−) had different degrees of toxicity, depending on the nanoparticle's localization inside the cell. For instance, the PNC(−) nanoparticles were not toxic to the H9c2 cardiac myocytes or the HEK293 kidney cells (Figure 8a,b), whereas they were toxic to the A549 lung carcinoma cells (Figure 8c). This can be explained by the minimal uptake of PNC(−) by normal cells, as opposed to the A549 cancer cells that exhibited enhanced nanoparticle uptake and localization to the lysosomes (Figure 5d−f and Figure 7c). ANC(+) also exhibited various degrees of toxicity. Notably, these nanoparticles were more toxic to H9c2, A549, and HEK 293 cells, since these cells exhibited increased nanoparticle internalization and lysosomal localization. Interesitingly, the breast cancer cells (MCF-7) did not show any toxicity after treatment with any of the nanoparticles studied, since these cells did not show any significant nanoparticle uptake. Incubation of the H9c2 and A549 cells with ANC(+) in the presence of inhibitors of endocytic pathway (2-deoxyglucose and sodium azide) abrogated the nanoparticle's cytotoxicity (Figure 9a,b), confirming that an endocytic uptake of these nanoparticles and eventual localization to lysosomes was responsible for their cellular toxicity. Taken together, these results demonstrate that localization of nanoceria into lysosomes (an acidic cell compartment), as opposed to localization into the cytoplasm, leads to
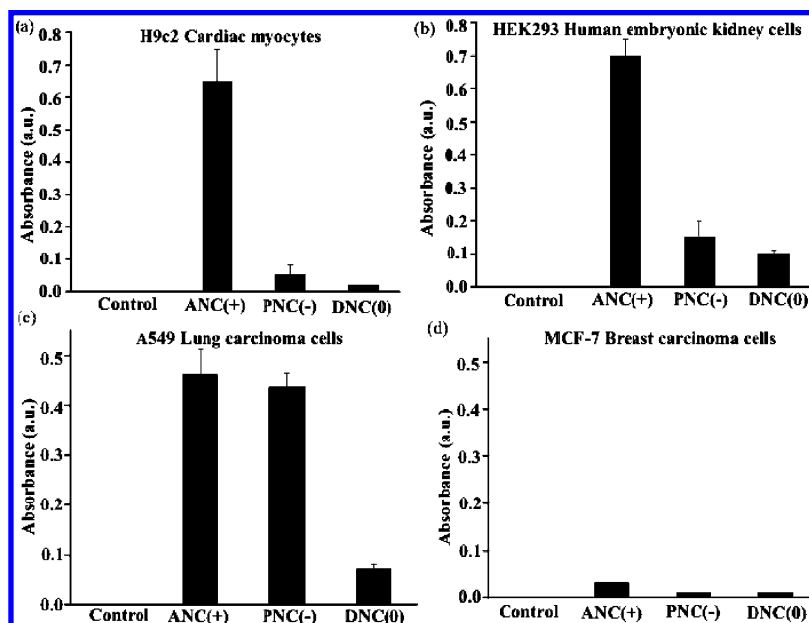

Figure 7. Lysosomal isolation and determination of the oxidase-like activity of the entrapped nanoceria. In H9c2 and HEK293 cell lines, the ANC(+) nanoparticles are mostly localized into lysosomes, judged by the presence of significant oxidase activity in the lysosomes isolated from these cell lines after incubation with ANC(+) (a and b). PNC(−) and DNC(0) treated H9c2 and HEK293 cells showed minimal oxidase activity in their lysosomes. In the A549 cell lines, oxidase activity was detected in cells treated with ANC(+) and PNC(−), while minimal activity was present in the DNC(0) treated cells (c). The lysomes isolated from MCF-7 cells did not show significant oxidase activity as the nanoceria did not internalized in these cells (d). Lysosomes isolated from nontreated cells do not show any oxidase activity as expected.
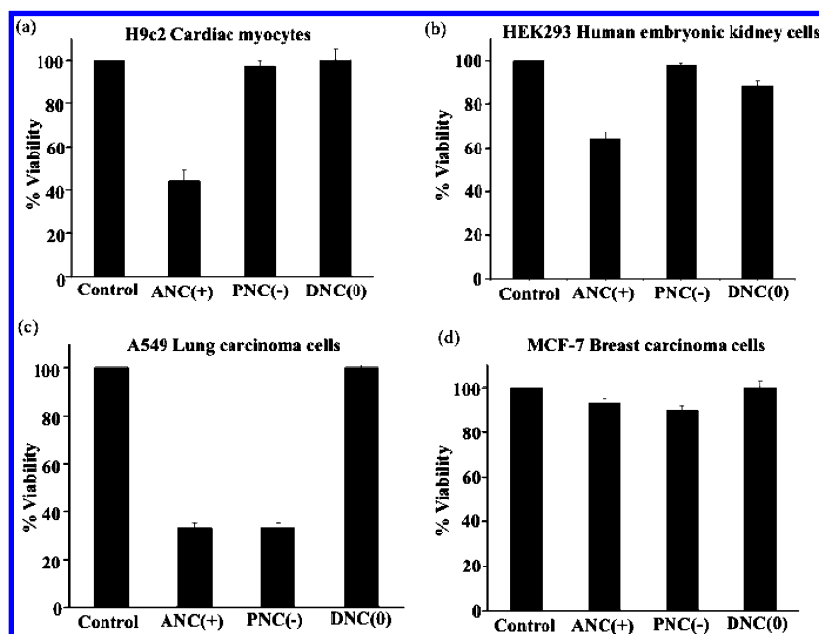
Figure 8. Cytotoxicity of cerium oxide nanoparticles. MTT assays show that the ANC(+) is cytotoxic to all cell lines except for the breast carcinoma cells. PNC(−) is only cytotoxic to A549 lung cancer cells as they internalize and localize into the lysosomes of these cells. DNC(0) does not show any toxicity to any of the cell lines.

cytotoxicity by activating the oxidase activity of nanoceria within these organelles.

Comparison of the Toxicity of Surface-Charge-Engineered Nanoceria and Iron Oxide Nanoparticles. To demonstrate that the observed cytotoxicity of nanoceria is attributed to the cerium oxide core (oxidase activity) and not to the nature of the polymeric coating, we performed experiments with DiI-labeled-aminated poly(acrylic acid) [IONP(+)] and DiI-labeled carboxylated poly(acrylic acid) [IONP(−)] coated iron oxide nanoparticles. Polymer-coated iron oxide nanoparticles have been widely used in various applications, particularly in magnetic resonance imaging (MRI) with minimal toxicity. For instance, various preparations of dextran-coated iron oxide nanoparticles are used in the clinic for liver and lymph node metastasis imaging.[27−29] Confocal microscopy studies of A549 and H9c2 cells incubated with these nanoparticles showed that IONP(+) were uptaken by the A549 lung carcinoma cells and H9c2 cardiac myocytes (Figure 10a,c), with a more punctuated internalization in the H9c2 cells, indicating lysosomal localization. In contrast, IONP(−) were not internalized

by both cells (Figure 10b,d). As expected, the polymeric iron oxide nanoparticles [IONP(+) and IONP(−)] were not toxic to either the nontransformed H9c2 cell line or the transformed A549 carcinoma cell line (Figure 11a,b). The fact that more of the IONP(+) nanoparticles were localized into the lysosomes upon internalization in H9c2 did not seem to significantly alter the toxicity profile of the polymer-coated iron oxide nanoparticles. These results are not surprising, as iron oxide nanoparticles do not possess oxidase activity, particularly at the low pH of the lysosomes. Therefore, we can conclude that the intrinsic oxidase behavior of cerium oxide nanoparticles is responsible for the nanoparticle's cytotoxicity, particularly when they localize into acidic cell compartments such as lysosomes. Cytotoxicity experiments with the neutral dextran-coated iron oxide nanoparticles were not performed since it is well established that these nanoparticles are nontoxic.[27−29]

DISCUSSION

The toxicity of nanomaterials depends on various factors, including the nature and chemical composi-
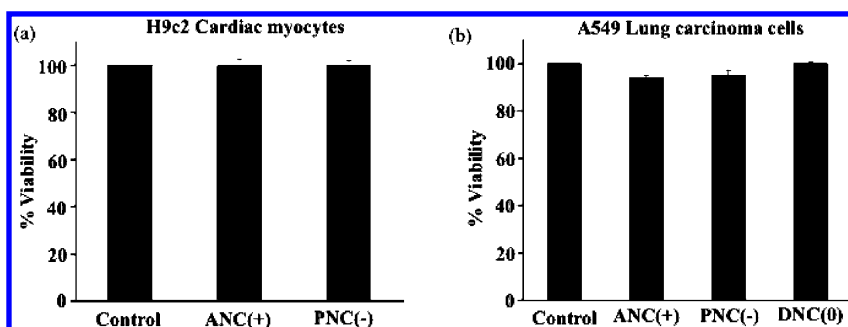

Figure 9. Cytotoxicity of cerium oxide nanoparticles in the presence of endocytosis inhibitors. Nanoparticles are not cytotoxic to either lung carcinoma or cardiac myocytes in presence of 2-deoxyglucose and sodium azide.
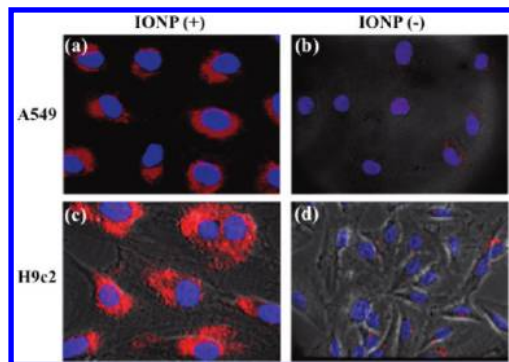
Figure 10. Uptake of carboxylated polymer-coated iron oxide nanoparticles [IONP(−)] and aminated polymer coated iron oxide nanoparticles [IONP(+)] by A549 and H9c2 cells. Confocal images of A549 and H9c2 cells after treatment with positively charged IONP(+) for 3 h show significant uptake of the nanoparticles (a and c). Meanwhile, no uptake of the negatively charged IONP(−) was observed in either A549 or H9c2 cells (b and d).

tion of the nanoparticle's core, mode of synthesis, size, shape, and crystallinity, surface reactivity, solubility in aqueous media, and degree of aggregation.[8,24] Although efforts have been made to study the effect of the polymeric surface coating and surface charge on the uptake, localization, and toxicity of nanomaterials, the mechanistic implications are still not completely understood. This is highly important as some nanomaterials, such as cerium oxide, may display either a beneficial (antioxidant) or toxic (oxidant) effect, depending on the pH of the compartment where they localize inside the cell. Here, we have shown that polymer-coated nanoceria displays different levels of toxicity, depending upon cellular uptake and subsequent subcellular localization. We have found that when polymer-coated nanoceria internalize and localize in the lysosomes, they become toxic due to the acidic microenvironment of these organelles, which activates the oxidase activity of nanoceria (Scheme 2). However, lower toxicity is observed when polymer-coated nanoceria localize into the cytoplasm of cells and are not internalized by the cells. Our results also show that the internalization, eventual localization, and cytotoxicity of polymer-coated nanoceria within the cell greatly depend on the surface charge of the polymeric coating and the

type of cell (cancerous *vs* normal). For instance, we have found that the aminated nanoceria [ANC(+)] were toxic to most of the cancer and normal cell lines studied, as these nanoparticles were uptaken and localized mostly into the lysosomes. This might indicate that nanoceria's intrinsic oxidant behavior at acidic pH is responsible for the observed cytotoxic of the cationic polymer-coated nanoparticles [ANC(+)]. Meanwhile, PNC(−) internalized mostly into the A549 lung carcinoma cells but not significantly into any of the other cell lines studied. This observation is corroborated by the fact that no lysosomal localization and therefore no toxicity is observed in MCF-7, H9c2 or HEK293 cells treated with PNC(−). In contrast, significant lysosomal localization and cytotoxicity is observed in the A549 cells treated with PNC(−). Surprisingly, distinct changes in cellular uptake were observed with the dextran-coated cerium oxide nanoparticles [DNC(0)]. A very disperse and diffused intracellular distribution was seen in all cell lines (cancer and normal) exposed to DNC(0), with very few of the DNC(0) localizing into the lysosomes. Therefore, the neutral DNC(0) nanoparticles were found to be nontoxic to any of the cell lines studied as they localize primarily in the cytoplasm. This suggests that the observed nontoxic behavior of DNC(0) might be attributed to its significantly low entrapment into lysosomes, contrary to ANC(+). On the basis of these results, DNC(0) would be a great platform for further development of therapeutic antioxidant nanoagents, as they exhibit minimal toxicity. In addtion, they can be effectively used in radiation therapy, since they are not toxic to normal cells. Also, as other dextran-coated nanoparticles have been found to have long circulation time,[27−29] similarly dextran-coated cerium oxide nanoparticles can be employed as long circulating antioxidant nanoagents.

Another factor that may contribute to the cytotoxic behavior of polymer-coated nanoceria is the type of cell line used and pH of the cell's microenvironment.[30−33] This is particularly relevant as tumor progression, increased invasion, metastasis, and acidic tumor environment have been found to be interrelated.[34−36] Differences between normal and tumor tissue and tumor-to-tumor variation may play a key
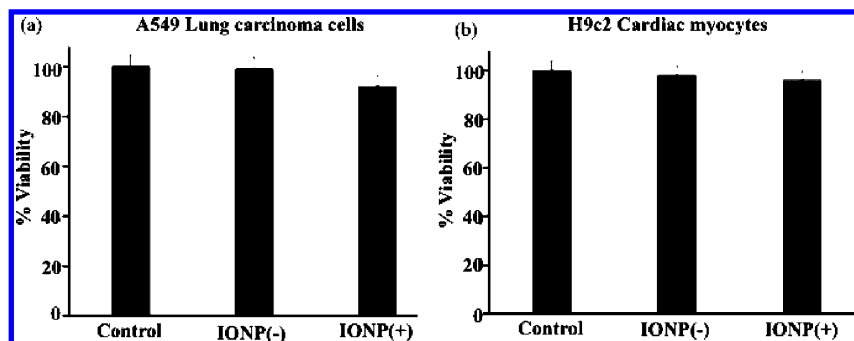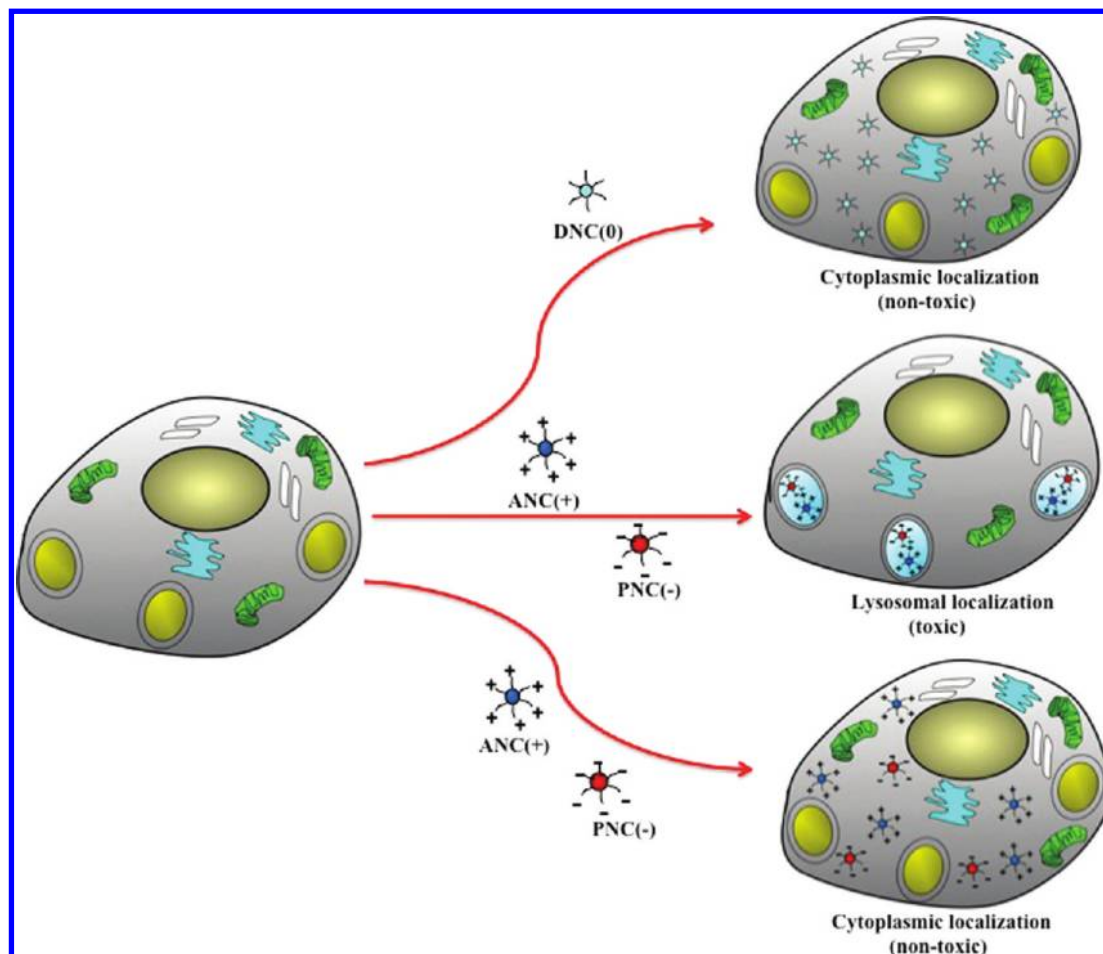

Figure 11. Cytotoxicity of carboxylated polymer coated iron oxide nanoparticles [IONP(−)] and aminated polymer coated iron oxide nanoparticles [IONP(+)] by A549 and H9c2 cells.

Scheme 2. Polymer-coated nanoceria's cell internalization, localization and proposed toxicity mechanism. Neutral DNC(0) internalized and localized mostly into the cytoplasm of cells and hence it is not cytotoxic. ANC(+) and PNC(−) can localize either into the cytoplasm or the lysosomes, depending on the type of cells. When the nanoceria localized to the lysosome, the low pH of this organelle activates the nanoparticle's oxidase-like activity, exhibiting toxicity. ANC(−) or PNC(+) that localized into the cytoplasm displayed no cytotoxicity

role in dictating the antioxidant *vs* oxidase behavior of the polymer-coated nanoceria. Previously, we have reported that polymer-coated nanoceria displays unique oxidase-like behavior at slightly acidic pH.[22] Therefore, in view of this oxidase-like property at acidic pH, intracellular distribution of the polymer-coated nanoceria into the lung carcinoma's lysosomes may be the reason for these nanoparticles' cytotoxicity. In addition, as A549 lung carcinoma cells and most tumors have been found to have upregulated glycolysis and increased lactic acid production,[30−33] this effect might further contribute toward the buildup of an acidic microenvironment, favoring nanoceria's oxidase activity and therefore sensitizing tumors toward radiation therapy. In summary, we believe that understanding the role of the polymer-coated nanoceria's surface charge and the influence that it has in the cell internalization, subcellular distribution, and differential antioxidant/oxidant activity will shed new light in delineating the mechanisms that lead to nanoceria's toxicity.

MATERIALS AND METHODS

Synthesis of Polymer-Coated Nanoceria Preparations [DNC(0), PNC(−), and ANC(+)]. The polymer-coated nanoceria preparations DNC(0) and PNC(−) were synthesized using the methodology described previously.[22] Briefly, a solution of cerium(III) nitrate (2.17 g, 1.0 M, Aldrich, 99%) in water (5.0 mL) was mixed separately with an aqueous solution of either poly(acrylic acid) (PAA, 0.5 M, Sigma) or dextran (1.0 M, Sigma) and mixed thoroughly using a vortex mixer. The resulting mixture was then added to an ammonium hydroxide solution (30.0 mL, 30%, Sigma Aldrich) under continuous stirring for 24 h at room temperature. The preparation was then centrifuged at 4000 rpm for two 30 min cycles to settle any debris and large agglomerates. The supernatant solution was then purified from free polymers and other reagents and then concentrated using a 30K Amicon cell (Millipore Inc.). ANC(+) was synthesized directly from PNC(−). In this method, PNC(−) (5.0 mL, 1.5 mg/mL) was treated with EDC [1-ethyl-3-(3-dimethylaminopropyl)carbodiimide] solution (28.0 mg, 30 mmol) in MES buffer (500 μL, 0.1 M, pH 6.0) followed by the dropwise addition of N-hydroxysuccinimide (NHS) solution (22.0 mg, 30 mmol) in MES buffer (500 μL, 0.1 M, pH 6.0) and incubated for 3 min at room temperature. Ethylenediamine (EDA, 10 mg, 25 mmol) in DMSO (100 μL) was then added dropwise to the final reaction mixture and the resulting mixture stirred for

an additional 3 h at room temperature. The resulting solution was purified to remove excess EDA and other reagents using an Amicon dialysis membrane (MWCO 30K) from Millipore. The final ANC(+) preparation (1.5 mg/mL) in DI water was stored in the refrigerator for further characterization.

DiI Encapsulation in Polymer-Coated Nanoceria [DNC(0), PNC(−), and ANC(+)]. In order to encapsulate the DiI dye (Invitrogen) into the polymeric matrix of the various polymer-coated nanoceria, we have used a modified solvent diffusion method, as reported previously.[23] Briefly, to 4.0 mL of the nanoparticle solution [1.5 mg/mL, DNC(0), PNC(−), or ANC(+)], was added dropwise 200.0 μL of DiI solution [6.0 μL of DiI (10 mg/mL) in 194 μL of DMSO] with mixing (1000 rpm) at room temperature. Afterward, the preparation was dialyzed (MWCO: 30K) against deionized water to remove any free DiI and finally was dialyzed overnight in phosphate-buffered saline (1X PBS) to reconstitute the final preparation in PBS.

Characterization. The various polymer-coated nanoceria preparations were characterized by transmission electron microscopy (TEM) to confirm the size of the nanocrystal core. TEM was performed by mounting a drop of nanoparticles on a holey carbon-coated copper 400-mesh grid (2SPI, USA), and images were taken on a FEI TECNAI F30 microscope operating at 300 kV. Surface charge on the nanoparticle was confirmed by ζ potential measurements (Malvern Zetasizer and disposable ζ cells). FT-IR experiments were performed on vacuum-dried samples to verify the surface functionalities on the nanoparticles (Perkin-Elmer Spectrum 100 FT-IR spectrometer). Fluorescence spectroscopy studies were done on DiI-labeled nanoceria using a Nanolog HORIBA JOBIN YVON spectrometer to confirm the DiI dye encapsulation in the nanoparticles.

Cell Culture. All cell lines in this study [lung carcinoma (A549), cardiac myocytes (H9c2), human embryonic kidney (HEK293), and breast carcinoma (MCF-7)] were obtained from ATCC. The cardiomyocytes were grown in Eagle's Minimal Essential medium supplemented with fetal bovine serum (10%), sodium pyruvate, L-glutamine, penicillin, streptomycin, amphotericin B, and nonessential amino acids. HEK293 cells were grown in Eagle's Minimal Essential medium supplemented with fetal bovine serum (10%) and 1% penicillin. The lung cancer cells were grown in Kaighn's modification of Ham's F12 medium (F12K) supplemented with 5% fetal bovine serum, L-glutamine, streptomycin, amphotericin B, and sodium bicarbonate. All cell lines were maintained at 37 °C, 5% CO$_2$ in a humidified incubator. MCF-7 cells were grown in Eagle's Minimal Essential medium supplemented with fetal bovine serum (10%) with 0.01 mg/mL bovine insulin and 1% penicillin.

Cellular Uptake of Polymer-Coated Nanoceria [DNC(0), PNC(−), and ANC(+)]. Ten thousand cells (cardiomyocytes, human embryonic kidney cells, lung carcinoma cells, and breast carcinoma cells) were seeded in Petri dishes and incubated with DiI-labeled DNC(0), DiI-labeled PNC(−), and DiI-labeled ANC(+) (1.0 mM) for 3 h at 37 °C, 5% CO$_2$ in a humidified incubator. Then, the cells were washed with 1X PBS and fixed with 10% formalin in 1X PBS. Afterward, the cells were incubated with DAPI (1 mg/mL, Molecular Probes) for 10 min. The cells were washed and visualized with a confocal microscope (Zeiss LSM 510).

Inhibition of Cellular Uptake of the Polymer-Coated Nanoceria. For these studies, 10000 cells (H9c2 and A549) were treated with the inhibitors sodium azide (10 mM) and 2-deoxyglucose (50 mM) for 30 min. Then, the cells were incubated with DiI-labeled PNC(−) and DiI-labeled ANC(+) preparations (1.0 mM) for 3 h at 37 °C, 5% CO$_2$ in a humidified incubator. Fixation and subsequent staining with DAPI were performed as described above. Experiments were done at 4 °C with incubation of the cells with the DiI-labeled PNC(−) and DiI-labeled ANC(+) preparations (1.0 mM) for 3 h.

Lysosomal Staining. After treatment of the corresponding cell lines with DiI-labeled DNC(0), DiI-labeled PNC(−), and DiI-labeled ANC(+) for 3 h, cells were washed and incubated for 20 min with Lysotracker (Invitrogen) (35 nM) at 37 °C, 5% CO$_2$ in a humidified incubator. Fixation procedures were performed as stated previously.

Lysosomal Isolation and Oxidase-Activity Determination of Entrapped Nanoceria. Lysosomes were isolated using a previously reported procedure described by Schroter et al.[37] Ten thousand cells (cardiomyocytes, human embryonic kidney cells, lung carcinoma cells, and breast carcinoma cells) were seeded in Petri dishes and incubated with ANC(+), PNC(−), and DNC(0) (1.0 mM) for 3 h at 37 °C, 5% CO$_2$ in a humidified incubator. Then, the cells were washed with 1X PBS, trypsinized, and centrifuged at 1000 rpm for 8 min. In order to isolate the lysosomes, cells were resuspended in an isotonic sucrose solution (1.0 mL, 0.08 M CaCl$_2$, 0.25 M sucrose, 10 mM Tris−HCl) to lyse the cells into cytosolic and organelles fractions and centrifuged at 25000g for 15 min. Subsequently, the supernatant was carefully removed, and the pellet was resuspended in 1.0 mL of 150 mM KCl (10 mM Tris−HCl, pH 7.4) followed by centrifugation at 25000g for 15 min to sediment the lysosomes. The pellet containing the lysosomes was resuspended in 200 μL of TMB (1.0 mg/mL) and incubated overnight at room temperature. After the incubation period, the absorbance at 652 nm of the lysosome suspension was recorded.

Cell Viability Assays. Cells (cardiomyocytes, human embryonic kidney cells, lung carcinoma cells, and breast carcinoma cells) were seeded in 96-well plates at a density of 3000 cells per well and incubated with ANC(+), PNC(−), and DNC(0) (1.0 mM) for 3 h. Then, 0.5 mM of MTT [3-(4,5-dimethylthiazol-2-yl)-2,5-diphenyltetrazolium bromide] (Sigma) was added, followed by incubation for 24 h. After 24 h, the resulting crystals were dissolved in 40 μL of acidified 2-propanol, and the absorbance at 570 nm was recorded using a plate reader (Bio-TEK, Synergy HT Multidetection Microplate reader).

REFERENCES AND NOTES

1. Weissleder, R. Molecular Imaging in Cancer. *Science* **2006**, *312*, 1168–1171.
2. Rosi, N. L.; Giljohann, D. A.; Thaxton, C. S.; Lytton-Jean, A. K. R.; Han, M. S.; Mirkin, C. A. Oligonucleotide-Modified Gold Nanoparticles for Intracellular Gene Regulation. *Science* **2006**, *312*, 1027–1030.
3. Lewin, M.; Carlesso, N.; Tung, C. H.; Tang, X. W.; Cory, D.; Scadden, D. T.; Weissleder, R. Tat Peptide-Derivatized Magnetic Nanoparticles Allow *In Vivo* Tracking and Recovery of Progenitor Cells. *Nat. Biotechnol.* **2000**, *18*, 410–414.
4. George, S.; Pokhrel, S.; Xia, T.; Gilbert, B.; Ji, Z. X.; Schowalter, M.; Rosenauer, A.; Damoiseaux, R.; Bradley, K. A.; Nel, A. E. Use of a Rapid Cytotoxicity Screening Approach To Engineer a Safer Zinc Oxide Nanoparticle through Iron Doping. *ACS Nano* **2010**, *4*, 15–29.
5. Xia, T. A.; Kovochich, M.; Liong, M.; Meng, H.; Kabehie, S.; George, S.; Zink, J. I.; Nel, A. E. Polyethyleneimine Coating Enhances the Cellular Uptake of Mesoporous Silica Nanoparticles and Allows Safe Delivery of siRNA and DNA Constructs. *ACS Nano* **2009**, *3*, 3273–3286.
6. Roiter, Y.; Ornatska, M.; Rammohan, A. R.; Balakrishnan, J.; Heine, D. R.; Minko, S. Interaction of Nanoparticles with Lipid Memberane. *Nano Lett.* **2008**, *8*, 941–944.
7. Vallhov, H.; Gabrielsson, S.; Stromme, M.; Scheynius, A.; Garcia-Bennett, A. E. Mesoporous Silica Particles Induce Size Dependent Effects on Human Dendritic Cells. *Nano Lett* **2007**, *7*, 3576–3582.
8. Nel, A. E.; Madler, L.; Velegol, D.; Xia, T.; Hoek, E. M.; Somasundaran, P.; Klaessig, F.; Castranova, V.; Thompson,

M. Understanding Biophysicochemical Interactions at the Nano-Bio Interface. *Nat. Mater.* **2009**, *8*, 543–557.

9. Schanen, B. C.; Karakoti, A. S.; Seal, S.; Drake, D. R., 3rd; Warren, W. L.; Self, W. T. Exposure to Titanium Dioxide Nanomaterials Provokes Inflammation of an *In Vitro* Human Immune Construct. *ACS Nano* **2009**, *3*, 2523–2532.

10. Shvedova, A. A.; Castranova, V.; Kisin, E. R.; Schwegler-Berry, D.; Murray, A. R.; Gandelsman, V. Z.; Maynard, A.; Baron, P. Exposure to Carbon Nanotube Material: Assessment of Nanotube Cytotoxicity using Human Keratinocyte Cells. *J. Toxicol. Environ. Health A* **2003**, *66*, 1909–1926.

11. Lam, C. W.; James, J. T.; McCluskey, R.; Hunter, R. L. Pulmonary Toxicity of Single-Wall Carbon Nanotubes in Mice 7 and 90 Days After Intratracheal Instillation. *Toxicol. Sci.* **2004**, *77*, 126–134.

12. Carlson, C.; Hussain, S. M.; Schrand, A. M.; Braydich-Stolle, L. K.; Hess, K. L.; Jones, R. L.; Schlager, J. J. Unique Cellular Interaction of Silver Nanoparticles: Size-Dependent Generation of Reactive Oxygen Species. *J. Phys. Chem. B* **2008**, *112*, 13608–13619.

13. Hussain, S. M.; Schlager, J. J. Safety Evaluation of Silver Nanoparticles: Inhalation Model for Chronic Exposure. *Toxicol. Sci.* **2009**, *108*, 223–224.

14. Chen, H. H. C.; Yu, C.; Ueng, T. H.; Chen, S. D.; Chen, B. J.; Huang, K. J.; Chiang, L. Y. Acute and Subacute Toxicity Study of Water-Soluble Polyalkylsulfonated C_{60} in Rats. *Toxicol. Pathol.* **1998**, *26*, 143–151.

15. Chen, H. H. C.; Yu, C.; Ueng, T. H.; Liang, C. T.; Chen, B. J.; Hong, C. C.; Chiang, L. Y. Renal Effects of Water-Soluble Polyarylsulfonated C60 in Rats with an Acute Toxicity Study. *Fullerene Sci. Technol.* **1997**, *5*, 1387–1396.

16. Nel, A.; Xia, T.; Madler, L.; Li, N. Toxic Potential of Materials at the Nanolevel. *Science* **2006**, *311*, 622–627.

17. Perez, J. M.; Asati, A.; Nath, S.; Kaittanis, C. Synthesis of Biocompatible Dextran-Coated Nanoceria with pH-Dependent Antioxidant Properties. *Small* **2008**, *4*, 552–556.

18. Chen, J. P.; Patil, S.; Seal, S.; McGinnis, J. F. Rare Earth Nanoparticles Prevent Retinal Degeneration Induced by Intracellular Peroxides. *Nat. Nanotechnol.* **2006**, *1*, 142–150.

19. Niu, J.; Azfer, A.; Rogers, L. M.; Wang, X.; Kolattukudy, P. E. Cardioprotective Effects of Cerium Oxide Nanoparticles in a Transgenic Murine Model of Cardiomyopathy. *Cardiovasc. Res.* **2007**, *73*, 549–559.

20. Tarnuzzer, R. W.; Colon, J.; Patil, S.; Seal, S. Vacancy Engineered Ceria Nanostructures for Protection from Radiation-Induced Cellular Damage. *Nano Lett.* **2005**, *5*, 2573–2577.

21. Korsvik, C.; Patil, S.; Seal, S.; Self, W. T. Vacancy Engineered Ceria oxide Nanoparticles Catalyze Superoxide Dismutase Activity. *Chem. Commun.* **2007**, 1056–1058.

22. Asati, A.; Santra, S.; Kaittanis, C.; Nath, S.; Perez, J. M. Oxidase-Like Activity of Polymer-Coated Cerium Oxide Nanoparticles. *Angew. Chem., Int. Ed.* **2009**, *48*, 2308–2312.

23. Santra, S.; Kaittanis, C.; Grimm, J.; Perez, J. M. Drug/Dye-Loaded, Multifunctional Iron oxide Nanoparticles for Combined Targeted Cancer Therapy and Dual Optical/Magnetic Resonance Imaging. *Small* **2009**, *5*, 1862–1868.

24. Verma, A.; Stellacci, F. Effect of Surface Properties on Nanoparticle-Cell Interactions. *Small* **2010**, *6*, 12–21.

25. Verma, A.; Uzun, O.; Hu, Y.; Hu, Y.; Han, H. S.; Watson, N.; Chen, S.; Irvine, D. J.; Stellacci, F. Surface-Structure-Regulated Cell-Membrane Penetration by Monolayer-Protected Nanoparticles. *Nat. Mater.* **2008**, *7*, 588–595.

26. Hu, Y.; Litwin, T.; Nagaraja, A. R.; Kwong, B.; Katz, J.; Watson, N.; Irvine, D. J. Cytosolic Delivery of Membrane-impermeable Molecules in Dendritic Cells Using pH-Responsive Core-Shell Nanoparticles. *Nano Lett.* **2007**, *7*, 3056–3064.

27. Weissleder, R. Liver MR Imaging with Iron Oxides: Toward Consensus and Clinical Practice. *Radiology* **1994**, *193*, 593–595.

28. Harisinghani, M. G.; Barentsz, J.; Hahn, P. F.; Deserno, W. M.; Tabatabaei, S.; van de Kaa, C. H.; de la Rosette, J.; Weissleder, R. Noninvasive Detection of Clinically Occult Lymph-Node Metastases in Prostate Cancer. *N. Engl. J. Med.* **2003**, *348*, 2491–2499.

29. Harisinghani, M. G.; Saksena, M. A.; Hahn, P. F.; King, B.; Kim, J.; Torabi, M. T.; Weissleder, R. Ferumoxtran-10-Enhanced MR Lymphangiography: Does Contrast-Enhanced Imaging Alone Suffice for Accurate Lymph Node Characterization. *Am. J. Roentgenol.* **2006**, *186*, 144–148.

30. Brahimi-Horn, M. C.; Chiche, J.; Pouysségur, J. Hypoxia Signalling Controls Metabolic Demand. *Curr. Opin. Cell Biol.* **2007**, *19*, 223–229.

31. Kim, J. W.; Dang, C. V. Cancer's Molecular Sweet Tooth and the Warburg Effect. *Cancer Res.* **2006**, *66*, 8927–8930.

32. Smith-Jones, P. M.; Solit, D.; Afroze, F.; Rosen, N.; Larson, S. M. Early Tumor Response to Hsp90 Therapy Using HER2 PET: Comparison with 18F-FDG PET. *J. Nucl. Med.* **2006**, *47*, 793–796.

33. Wu, M.; Neilson, A.; Swift, A. L.; Moran, R.; Tamagnine, J.; Parslow, D.; Armistead, S.; Lemire, K.; Orrell, J.; Teich, J.; et al. A Multiparameter Metabolic Analysis Reveals a Close Link Between Attenuated Mitochondrial Bioenergetic Function and Enhanced Glycolysis Dependency in Human Tumor Cells. *Am. J. Physiol. Cell Physiol.* **2007**, *292*, C125–136.

34. Raghunand, N.; Mahoney, B.; van Sluis, R.; Baggett, B.; Gillies, R. J. Acute Metabolic Alkalosis Enhances Response of C3H Mouse Mammary Tumors to the Weak Base Mitoxantrone. *Neoplasia* **2001**, *3*, 227–235.

35. Rofstad, E. K.; Mathiesen, B.; Kindem, K.; Galappathi, K. Acidic Extracellular pH Promotes Experimental Metastasis of Human Melanoma Cells in Athymic Nude Mice. *Cancer Res.* **2006**, *66*, 6699–6707.

36. Stubbs, M.; McSheehy, P. M.; Griffiths, J. R. Causes and Consequences of Acidic pH in Tumors: A Magnetic Resonance Study. *Adv. Enzyme Regul.* **1999**, *39*, 13–30.

37. Schroter, C. J.; Braun, M.; Englert, J.; Beck, H.; Schmid, H.; Kalbacher, H. A Rapid Method to Separate Endosomes from Lysosomal Contents Using Differential Centrifugation and Hypotonic Lysis of Lysosomes. *J. Immunol. Methods* **1999**, *227*, 161–168.

ARTICLE